ARTICLE OPEN

Check for updates

Molybdenum effects on the stability of passive films unraveled at the nanometer and atomic scales

Vincent Maurice[1]✉ and Philippe Marcus[1]✉

Data recently obtained on model FeCrNi(Mo), 316 L stainless steel, and FeCrNiCo(Mo) passivated surfaces by advanced surface analysis and density functional theory modeling are comprehensively discussed to unravel the multiple effects that molybdenum might have at the nanometer and atomic scales to enhance the stability of passive films. The key role played on corrosion protection by the compositional and structural nanoscale defects of the passive film that originate from the pre-passivation mechanisms of the surface is considered. It is shown how Mo, enriched together with Cr in the nanometer-thick passive film, can combine several effects to enhance the resistance to Cl^--induced passivity breakdown. Enriched as Mo(VI) species in the outer exchange layer of the passive film, Mo impedes the deep penetration of Cl^- ions and limits their access to the inner barrier layer. Dispersed as Mo(IV) at the interface with the inner layer, Mo protects against the entry of Cl^- ions into the defect sites of the Cr(III) oxide barrier. Present as Mo(IV + δ) in the Fe-rich compositional nanoscale defects self-generated by the local failure of Cr supply upon initial formation of the barrier layer, Mo enhances the selective dissolution of iron and its replacement by chromium and molybdenum. By impeding the formation of O vacancies, Mo also increases the resistance against chloride entry in the oxide matrix, thereby curing these the Fe-rich weak sites against Cl^--induced passivity breakdown.

npj Materials Degradation (2024)8:3 ; https://doi.org/10.1038/s41529-023-00418-6

INTRODUCTION

Passivity is the best of all means of corrosion protection of metals and alloys components in service conditions[1–7]. However, the presence of aggressive anions such as chloride ions in the environment can trigger the initiation of localized corrosion and thereby limit the durability of the self-protection property of the metallic substrate[8–14].

On stainless steels (SS) and Ni-based stainless alloys, chromium is the key alloying element added to obtain corrosion protection by passivity. Chromium is enriched in the passive film[15–25], and it is protective owing to the formation of Cr(III) oxidized species with extremely low dissolution kinetic[26]. Compared to air-formed native oxide films, chromium (and molybdenum for Mo-bearing alloys) is further enriched in the passive oxide film when the alloy substrate is immersed in acidic and near-neutral aqueous environments due to the faster dissolution of iron species in the electrolyte[16,19,20,22,27,28]. Anodic passivation causes re-growth and dehydrogenation of the oxide film when compared to open circuit (i.e., free) potential conditions[22,23]. The passive oxide films are 1 to 3 nm-thick, depending on alloy composition and passivation conditions[20–22,24,29,30]. Thinning or thickening can also be observed after passivation, depending on the competition between the rates of oxide dissolution and oxide re-growth[22–24]. The alloy close to the metal/oxide interface exhibits a modified composition, resulting from the preferential oxidation of elements such as chromium[31] with higher affinity to oxygen during oxide film formation and leading to enrichment in metallic nickel under the oxide layer in Fe-based austenitic alloys[17,21,22,24,32].

In many of the surface analytical studies of passivated stainless steels and alloys, the stratified structure of the nanometer-thick passive film could be characterized. It is described by a bilayer model[21,22,24,28,29]. The inner layer forms a dense oxide barrier highly enriched in Cr(III) oxide, limiting atomic transport across the interface and thus giving the alloy its high corrosion resistance. The outer layer, viewed as the exchange layer with the electrolyte, can contain Cr(III) hydroxide, Fe(II,III) oxide/hydroxide, Ni(II) hydroxide, and Mo(IV,VI) oxide species depending on the alloy composition[21–24,28–30]. Since the formation of oxide is usually faster compared to cation diffusion, the possible occurrence of a non-equilibrium solute capture has been suggested[33–35], defined as a non-stoichiometric Cr(III) oxide matrix in which Ni^{2+}, Fe^{2+} as well as Mo^{4+} cations would be captured.

In addition to chromium, molybdenum is the other key alloying element added in stainless alloys for improving the corrosion resistance. Other elements such as N can also be added[36,37]. Mo added in stainless steel can enhance significantly the resistance to pitting, crevice and stress corrosion[38]. For 316 L and 304 L austenitic stainless steels of quite similar composition, the 2 at. % Mo added in grade 316 L markedly improve the resistance to chloride-induced pitting corrosion[39], and it has been shown that 1.5 at. % Mo added in FeCrNi alloys can decrease the active dissolution rate in HCl aqueous solution by a factor of 5 to 10[40,41]. Besides, sodium molybdate is also widely used as a corrosion inhibitor[42–44], and it has been argued that adding molybdenum to stainless steels would be like adding a molybdate inhibitor to the solution[45,46].

Despite many studies, the exact role that molybdenum plays in stabilizing passivity is still debated. Some authors say that it aids in preventing the breakdown of the passive film in the first place[39,47–49], while for others molybdenum would reduce active dissolution after passivity breakdown and thus promote the self-repair of the oxide film[40,50–54]. These mechanisms may act solely or concurrently to conduce to the enhancive effect of Mo on corrosion resistance depending on how advanced is the localized corrosion process[14,55].

The view that Mo mitigates passivity breakdown is supported by results showing that Mo species impede the penetration of

[1]PSL University, Chimie ParisTech—CNRS, Institut de Recherche de Chimie Paris, Physical Chemistry of Surfaces Group, 11 rue Pierre et Marie Curie, 75005 Paris, France.
✉email: vincent.maurice@chimieparistech.psl.eu; philippe.marcus@chimieparistech.psl.eu

aggressive ions such as Cl^- into the oxide film. Indeed, Mo(IV,VI) and Cr(III) oxide species are found to be concentrated mostly in the outer exchange and inner barrier layers of the duplex passive film, respectively[21–24,28–30,56,57], and the penetration of Cl^- can be limited to only the outmost part of the oxide film[57]. Also, Cl^--incorporated islands were reported to form on the surface of 316 L SS with no Cl^- penetration underneath after immersion in NaCl aqueous solution, while no islands but pits were formed on 304 L SS immersed in the same solution[58]. Besides, the presence of Mo oxides on the surface would prevent the outward diffusion of Cr to the oxide surface[59], thus preventing the voiding mechanisms proposed as one route leading to passivity breakdown[8–13]. Mo oxides would also suppress the passive film dissolution[60], which is another route that can lead to passivity breakdown[8–13].

In support of the view that Mo promotes self-repair, it has been argued that, although a certain amount of Cr is necessary to ensure the beneficial effect of Mo in increasing the corrosion resistance[30], the Mo surface coverage on FeCrMo alloy is small and yet active dissolution is markedly decreased[40,41]. On Ni-based alloy surfaces, it was observed that Mo enriches at the surface in the transpassive range, and redissolves when the potential is returned to the passive range, suggesting that Mo dissolution/precipitation could play an important role in the breakdown/repassivation process[61], possibly involving the formation of molybdates[55].

Herein, we comprehensively discuss data recently obtained on FeCrNi(Mo) model alloy, on 316 L stainless steel, and on Cr- and Mo-bearing multi-principal element alloy (MPEA) passivated surfaces using scanning tunneling microscopy (STM), X-Ray photoemission spectroscopy (XPS) and time-of-flight secondary ion mass spectrometry (ToF-SIMS). The discussion highlights the key role played on corrosion protection by the compositional and structural defects of the passive film that originate from the pre-passivation mechanisms of the surface. Data obtained from density functional theory (DFT) modeling are also included in the discussion as they contribute to unravel the multiple effects that molybdenum might have at the nanometer and atomic scales to enhance the stability of passive films.

RESULTS AND DISCUSSION

Fe-rich nanoscale defects in Cr oxide barrier layers

The detailed mechanisms by which an oxide film initially forms on a metal substrate until complete surface saturation, i.e., how the surface pre-passivates, can determine the corrosion protection properties of the substrate in its later life. However, for reactive materials such as Fe- or Ni-based stainless alloys, the formation of the native oxide layer is so fast that extremely well-controlled conditions of exposure to the oxidizing environment are required to be able to time-resolve the transition of the surface state from oxide-free to native oxide-covered. On austenitic stainless steel, this was achieved by applying a surface science approach in which a model single crystalline surface, FeCrNi(100), was first cleaned from any residual traces of surface oxide and contamination in ultra-high vacuum (UHV) and then exposed stepwise to gaseous oxygen at ultra-low pressure until saturation of the oxide growth. In situ chemical and structural surface analysis by XPS and STM was applied at each step, including to verify initial surface cleanliness and structure after preparation[62–64]. The work provided direct evidence that the surface oxide film contains nanoscale heterogeneities of composition and structure, even when grown on a substrate of well-controlled crystallographic orientation and free of emergent microstructure defects, owing to the mechanisms of local supply of chromium (Fig. 1).

In the ultra-early stage of oxidation (which would correspond to a few nanoseconds at atmospheric pressure), local nucleation of chromium oxide was observed at the step edges[62,63] at moderate temperature (250 °C). Chromium is supplied by atomic pumping from the terraces to the step edges for formation of Cr(III)-rich oxide nuclei, via a Cr surface diffusion process involving surface vacancies. With ongoing exposure to oxygen, the formation of Fe-rich oxide nuclei is favored at locations adjacent to the step edges, where Cr was locally depleted owing to its initial consumption to form chromium oxide nuclei. Subsequently, a Cr(III)-rich layer nearly saturating the surface is formed, involving Cr (and Fe) transport from the metallic planes below the oxide. However, nearby the step edges, three-dimensional Fe-rich oxide islands, initiated owing to local depletion of Cr, continue to grow.

At room temperature[64], nucleation of Fe oxide occurs at the defect sites on the terraces while Cr(III) oxide nucleation occurs at the step edges. With ongoing exposure to oxygen, the oxide nuclei grow to grain size of up to 2–3 nm and in density until saturation of the surface by a nanogranular film homogeneously covering the substrate terraces and step edges. Oxide nuclei and nanograins develop no well-ordered structure, unlike at higher temperature (250 °C) where crystalline films are formed. A Cr(III)-rich oxide film is formed at saturation with a Cr(III) to Fe(II/III) ratio depending on the local supply of metallic Cr and Fe during nucleation and growth and resulting in compositional heterogeneity at the nanoscale of the granular morphology. At 250 °C, the compositional heterogeneity of the surface oxide is less densified at the nanoscale owing to the higher temperature promoting atomic transport and thus the space separation of the formation of oxide nuclei enriched in either of the elements. Regardless of the temperature, nickel does not enter the composition of the grown oxide films.

To our knowledge, no similar local analysis of the nucleation and growth mechanisms has been conducted with model single-crystal surfaces of Mo-bearing stainless steel. However, in situ XPS analysis of the nucleation and growth process on (100)-oriented FeCrNiMo single-crystal surfaces using the same approach revealed that initial oxidation of molybdenum occurs after chromium and iron have already begun to oxidize and confirmed that no nickel was found in an oxidized form within the oxide film[65]. From angular XPS analysis, in which the relative intensities of the species are measured at varying take-off angle of the photoelectrons, thus varying the depth sensitivity of the collected information, Cr(III) and Fe(II) were found enriched closer to the modified alloy–oxide interface with Fe(III) found predominantly at the outer part of the film. Oxidized molybdenum was found as both Mo(IV) and Mo(VI).

Despite the unknown, and yet to be studied, effects of water vapor on the nucleation and growth process, these studies performed on model stainless steel surfaces allow us to better understand the nature and the mechanisms of formation of native surface oxides. They provide us a nanoscale insight that needs to be considered to discuss the impact of the local chemical and structural defects self-generated by the initial oxidation process on the corrosion protection and the initiation of localized corrosion. Indeed, based on this insight, passivity breakdown can be expected in the least Cr(III)-enriched regions of the protective surface oxide, i.e., the Fe-rich defect sites in the passive film, and self-repair can be expected to be ineffective in the metallic surface regions depleted in Cr.

Passivation-induced alterations of native oxide films

Corrosion being observed in water-containing environments, it is a prerequisite to study the alterations of the oxide film initially formed on the surface when exposed to an aqueous electrolyte. This can be done by controlling the initial oxidation conditions and then exposing the native oxide-covered surface to the electrolyte of interest at open circuit potential (OCP) to investigate the naturally formed passive film. Additionally, the interface can be polarized in the passive range to study the alterations brought

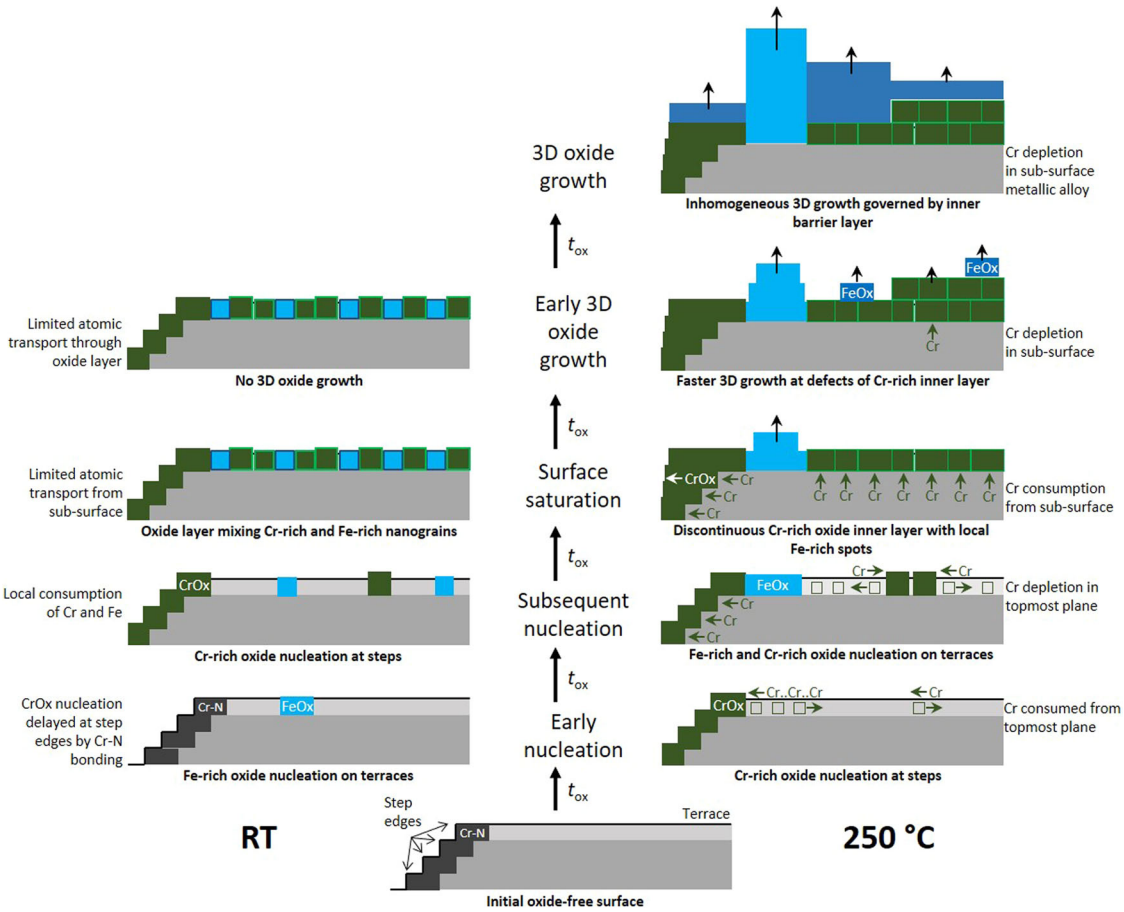

Fig. 1 Early oxidation mechanisms at the origin of the nanoscale heterogeneity of the surface oxide film grown on austenitic stainless steel. Cross-section comparative models at room temperature (RT) and 250 °C with height-to-width aspect ratio not to scale.

by anodic polarization. In order to limit the possible artefacts brought by ex situ transfer for surface analysis, a closed system, with direct transfer avoiding exposure to ambient air between UHV analytical platform for surface preparation and analysis and Ar-filled chamber or glove box equipped for electrochemical treatment and measurement can be used[6,15,20,22,23,25]. Alternatively, in situ conditions can be studied with specifically-designed electrochemical cells and using the benefits of synchrotron-emitted photons for surface analysis, e.g., by near-ambient XPS[66].

Using the first approach[22,23], it has been shown that on a 316 L SS surface covered by the native oxide spontaneously formed after mechanical polishing and immersed in sulfuric acid solution (selected as model chloride-free corrosive aqueous electrolyte), the passivation mechanism is characterized by faster dissolution of oxidized iron already occurring at free potential (OCP). The thickness of the initial native oxide film decreases; however, its enrichment in Cr(III) and Mo(IV,VI) is promoted, mostly in the exchange outer hydroxide layer of the duplex structure (Fig. 2). Anodic polarization in the passive range causes the steady-state thickness to increase owing to oxide growth less rapidly balanced by oxide dissolution than at OCP. The inner barrier oxide layer of the passive film becomes thicker, reflecting the increase of the enrichment in Cr(III) oxide, while the outer exchange layer is less Cr(III) hydroxide-rich, but maintains the Mo(IV/VI) enrichment obtained at OCP. Metallic Mo concentration is unaltered in the modified alloy region underneath the oxide film compared to the initial surface state.

On a pre-oxidized surface obtained by exposing the oxide-free 316 L SS surface prepared under UHV to low oxygen pressure at room temperature[23], the oxide film grown at saturation is thinner than on the native oxide-covered surface due to minimization of the promoting effect of water on the surface oxidation kinetics (Fig. 2). The formation of the inner layer is limited to less than one equivalent monolayer (i.e., not continuous) and the outer layer is thinner but equally enriched in Mo(IV,VI) than on the native oxide-covered surface. Mo concentration is unaltered in the modified alloy region underneath the oxide film. At OCP, faster dissolution of oxidized iron also promotes the Cr(III) and Mo(IV,VI) enrichment. However, molybdenum enrichment is markedly increased in the exchange outer layer compared to the native oxide-covered surface, which improves the protectiveness against transient active dissolution during the transition from OCP to anodic passive state[23]. Like on the native oxide-covered surface, anodic passivation increases the steady-state thickness but with higher Mo-enrichment in the exchange outer layer.

On (100)-oriented FeCrNiMo single-crystal surfaces[25], thermal pre-oxidation at low oxygen pressure and 250 °C was also found to improve the protectiveness of the surface oxide film during the OCP-to-anodic passive state transition when compared with the native oxide formed on the same surface. The thermal oxide film was found to be enriched in iron which later dissolved into the acidic electrolyte after being held at OCP, resulting in the enrichment of chromium and molybdenum in the film like on 316 L SS surfaces. Anodic passivation causes growth of the film and favors dehydrogenation of both chromium and molybdenum. Thermal pre-oxidation at low oxygen pressure promotes the enrichment of molybdenum in the passive film, albeit not as significantly when compared to room temperature pre-oxidation on 316 L SS surfaces. However, it enhances the growth of the chromium inner oxide layer after anodic passivation, which can be

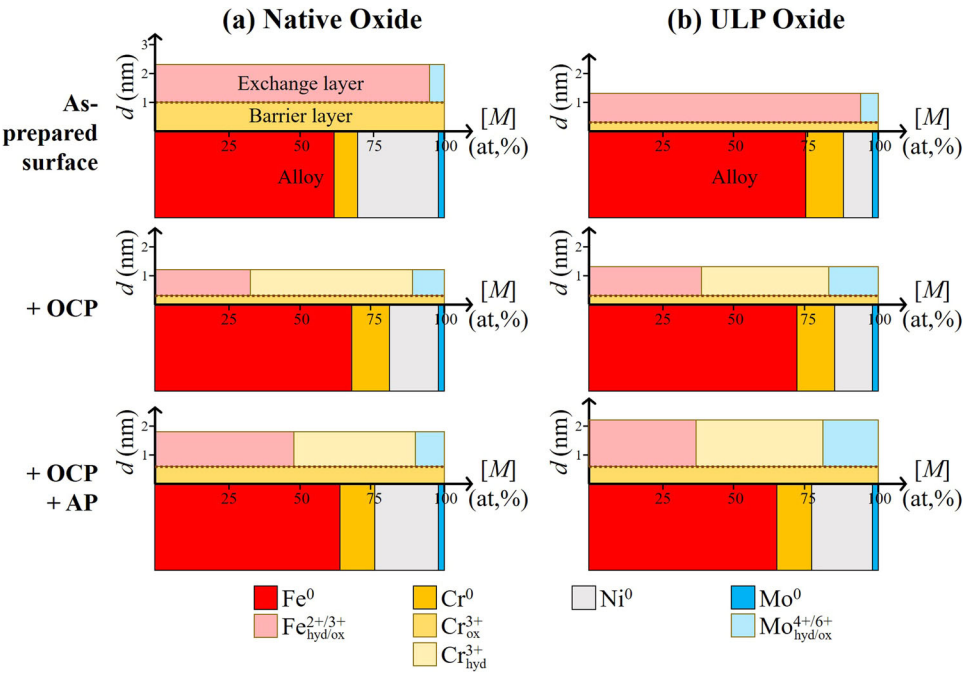

Fig. 2 Equivalent thickness (nm) and relative concentration (at. %) of the surface oxide films and modified alloy regions of 316 L SS surfaces as calculated from XPS data using a bilayer model of photoelectron intensity attenuation. a native oxide-covered surface; **b** surface pre-oxidized at ultra-low pressure (ULP) of oxygen sequentially treated at open circuit potential (OCP) and under anodic polarization (AP) in 0.05 M H_2SO_4. Reproduced from ref. [23]. Copyright owned by authors.

expected to influence the transport of ions through the passive film.

Owing to their local nature and nanometer dimensions, it is extremely difficult to investigate the fate of the Fe-rich weak sites of protection initially generated in the barrier layer of the surface oxide film upon natural passivation at free potential and/or anodic passivation. However, we can reasonably speculate based on the insight brought by the studies of the global alterations induced by passivation. Iron oxides dissolving faster, it can be inferred that the Fe-rich defect sites of inner barrier layer may dissolve already at OCP, at least partially. Thereby, their content in iron would decrease, as well as their density in the inner layer in case of complete dissolution. Upon re-growth of the oxide film under anodic polarization, iron in these Fe-rich defect sites of the inner barrier layer would be replaced mostly by chromium but possibly also by molybdenum observed to be globally further enriched in the passive films. While the enrichment in Cr(III) oxide is directly reflected by the increase in thickness of the barrier layer (assumed to be 100% Cr(III) oxide in the quantification models), the enrichment in Mo(IV,VI) species is localized in the outer layer of these models. However, detailed analysis of the depth distribution of molybdenum in the protective oxide films shows that it is also present deeper, in the inner barrier layer in the protective oxide film as discussed below.

Passivity enhancement by Mo (and Cr) enrichment

Controlling the pre-oxidation conditions appears instrumental to promote the surface molybdenum enrichment of the initial surface oxide, as shown on model FeCrNiMo and 316 L SS surfaces, which can be expected to benefit the sealing properties of the exchange outer layer of the passive film against the ingress of aggressive ions. Moreover, the Fe-rich weak sites of the inner barrier layer would be healed by mostly Cr but also Mo replacement. Besides, the re-passivation properties of the modified alloy region after passivity breakdown would not be altered since molybdenum is not depleted in this region. Beneficial effects on passivity breakdown and self-repair were indeed observed on 316 L SS surfaces prepared by a surface finishing pretreatment of vibratory polishing[67]. XPS and ToF-SIMS surface analysis confirmed that the vibratory finishing pretreatment increases the Cr and Mo enrichments in the native oxide film. As a result, the bilayer structure was characterized by a thicker Cr(III) oxide inner barrier layer and a more Cr(III) hydroxide- and Mo(IV,VI) oxide-enriched outer exchange layer than on the surface prepared by traditional mechanical polishing. Accelerated testing of the resistance to passivity breakdown and the initiation of localized corrosion was performed by potentiostatic polarization in the passive range, first in chloride-free aggressive acidic electrolyte (0.05 M H_2SO_4 (aq)) until reaching a quasi-steady-state of passivity, and then by sequentially increasing the chloride ions (NaCl) concentration without changing the pH.

Several beneficial effects of the Mo (and Cr) enrichment of the native oxide-covered surface could thus be highlighted (Fig. 3a). Vibratory finishing of the surface was found to enhance passivity, as shown by the lower current density observed in the Cl-free solution at the active/passive transition and in the near steady-state of passivity compared to a surface finish by traditional polishing, which can be assigned to the initial higher Cr enrichment of the surface. Resistance to chloride-induced passivity breakdown was also improved, as shown by a lower frequency of breakdown/self-repair events, i.e., metastable pitting, observed for the more Mo-rich vibratory polished surface. It can be noticed that despite being less frequent the metastable events are of higher amplitude for the vibratory polished alloy implying that the surface re-passivates despite the possible formation of larger metastable pits. Furthermore, a higher chloride concentration was needed to trigger stable pitting/crevice corrosion, and thus to block the self-repair of passivity on the more Mo-rich vibratory polished surface. Thus, with such an accelerated test, it was shown that the initial Mo enrichment of the native oxide-covered surface can act concurrently to enhance the stability of the passive state, by increasing the resistance to Cl-induced breakdown of the passive film, and by mitigating the blocking

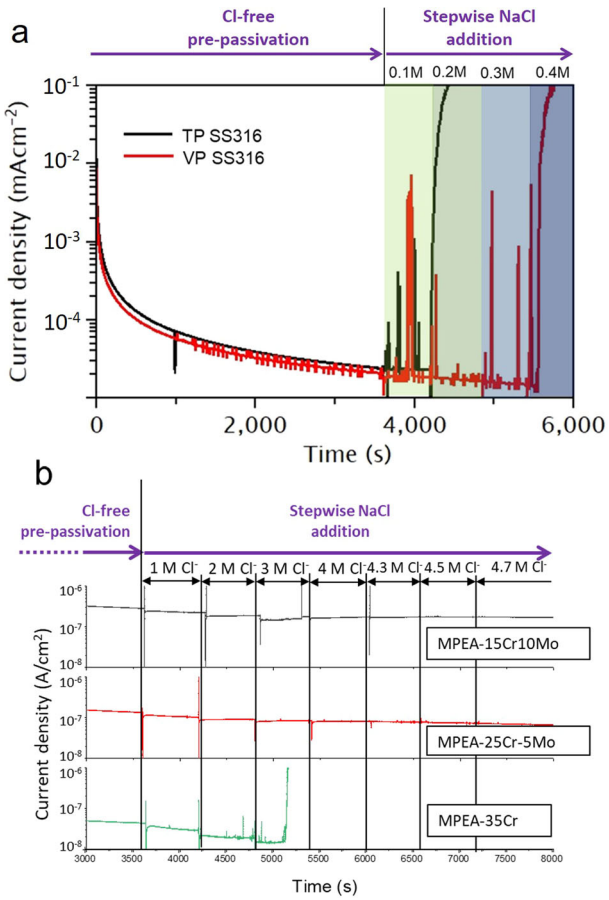

Fig. 3 Accelerated testing of resistance to passivity breakdown and initiation of localized corrosion. a 316 L SS samples prepared by traditional polishing (TP) and vibratory polishing (VP); **b** $Cr_{15}Fe_{10}Co_5Ni_{60}Mo_{10}$ (MPEA-15Cr10Mo), $Cr_{25}Fe_{25}Co_5Ni_{40}Mo_5$ (MPEA-25Cr5Mo) and $Cr_{35}Fe_{20}Co_5Ni_{40}$ (MPEA-35Cr) samples prepared by traditional polishing. Passivation current transients were recorded in 0.05 M H_2SO_4(aq) after stabilization at OCP. Samples were polarized at (**a**) +0.3 V/SHE and (**b**) +0.64 V/SHE in the Cl-free base electrolyte before stepwise increasing the NaCl concentration as marked. Adapted from references (**a**)[67] and (**b**)[69]. Copyright owned by authors.

effect of chloride ions on the re-passivation of the metallic surface exposed by the passive film breakdown.

These enhancing effects of molybdenum on the passivity of stainless steel were confirmed by investigating the corrosion properties of Cr- and Mo-bearing multi-principal element alloys of higher Mo content than 316 L SS[68]. Such alloys ($Cr_{25}Fe_{25}Co_5Ni_{40}Mo_5$, $Cr_{15}Fe_{10}Co_5Ni_{60}Mo_{10}$ in at. %) were designed, processed and characterized as having a single phase *fcc* structure that is maintained while varying their relatively high content in Cr and Mo. It was confirmed by ToF-SIMS and XPS surface analysis that the native oxide films had a bilayer structure with the inner barrier layer mostly consisting of Cr(III) oxide, and the outer exchange layer containing Cr(III) hydroxide, Fe(II,III) oxide/hydroxide and Ni(II) hydroxide[69]. As detailed further on, Mo was enriched as Mo(IV,VI) oxide species, and mostly concentrated in the outer layer, like on stainless steel.

Submitted to the same type of accelerated corrosion test as 316 L SS (Fig. 3b), the beneficial effect of Cr in enhancing passivity was confirmed, as observed by the near steady-state passive currents decreasing in the Cl-free solution with increasing Cr content in the substrate. For an Mo-free MPEA ($Cr_{35}Fe_{20}Co_5Ni_{40}$), Cl-induced metastable pitting was followed by the initiation of

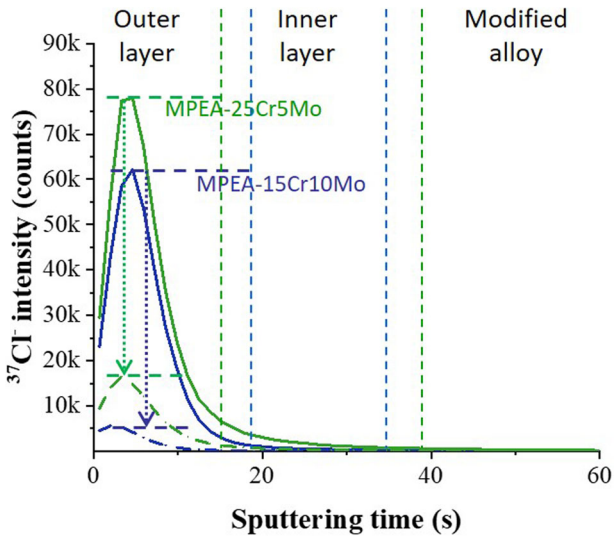

Fig. 4 In-depth distribution of chloride ions on passivated $Cr_{15}Fe_{10}Co_5Ni_{60}Mo_{10}$ (MPEA-15Cr10Mo) and $Cr_{25}Fe_{25}Co_5Ni_{40}Mo_5$ (MPEA-25Cr5Mo) surfaces as measured by ToF-SIMS. Samples were passivated in 0.05 M H_2SO_4 + 4.7 M NaCl at 0.64 V/SHE for 1 h with (broken line) or without (plain line) pre-passivation in the NaCl-free electrolyte. The margin of error for the maximum and interface Cl^- signal intensities is smaller than 5%. Adapted from ref. [70]. Copyright owned by authors.

localized corrosion despite the high content of the alloy in Cr (35 at. %). In contrast, for both Mo-bearing MPEAs, no passivity breakdown/self-repair events were observed as well as no initiation of localized corrosion, even for a chloride concentration as high as 4.7 M. Like in Cl-free solution, the near steady-state passive currents were even observed to continuously decrease with time, showing no Cl-induced degradation of the passive state.

To understand the absence of effect of chloride ions on passivated Mo-bearing MPEAs, the questions that arise are whether the Cl^- ions of the concentrated aggressive environment in these tests interact with the passivated surface or not, and, if yes, how deep they penetrate the protective oxide films. This was answered by applying ToF-SIMS to characterize the depth distribution of Cl from the outer surface of the passive film to the modified alloy region underneath (Fig. 4)[70]. Indeed, the Cl^- ions were found to interact with the passivated surface and penetrate the passive film. However, the penetration was limited to the outer layer of the bilayer structure. In the inner layer, no penetration was observed for the $Cr_{15}Fe_{10}Co_5Ni_{60}Mo_{10}$ MPEA and only trace penetration was observed for the $Cr_{25}Fe_{25}Co_5Ni_{40}Mo_5$ MPEA in the most severe conditions, i.e., without pre-passivation of the surface in Cl-free solution. On both alloys, penetration did not reach the metal substrate. This absence of Cl^- penetration until the interface with the substrate in the most severe tested conditions, whereas traces access the barrier inner layer, reflects the curing effect of Mo on the Fe-rich weak sites of the inner barrier layer.

Comparison of the two alloys shows that increasing the Mo content in the alloy and its enrichment in the outer layer of the passive film (about 30 and 17 Mo at. % for $Cr_{15}Fe_{10}Co_5Ni_{60}Mo_{10}$ and $Cr_{25}Fe_{25}Co_5Ni_{40}Mo_5$, respectively, as quantified by XPS analysis) decreases the amount of penetrated chorides (Fig. 4). Besides, pre-passivation in the Cl-free agressive solution also contributes to significantly impede the penetration of the agressive species whereas no compositional changes of the passive film were observed, which was assigned to a less defective nanostructure rather than to compositional enhancement of the passive films[70]. Hence, Mo can be viewed as having

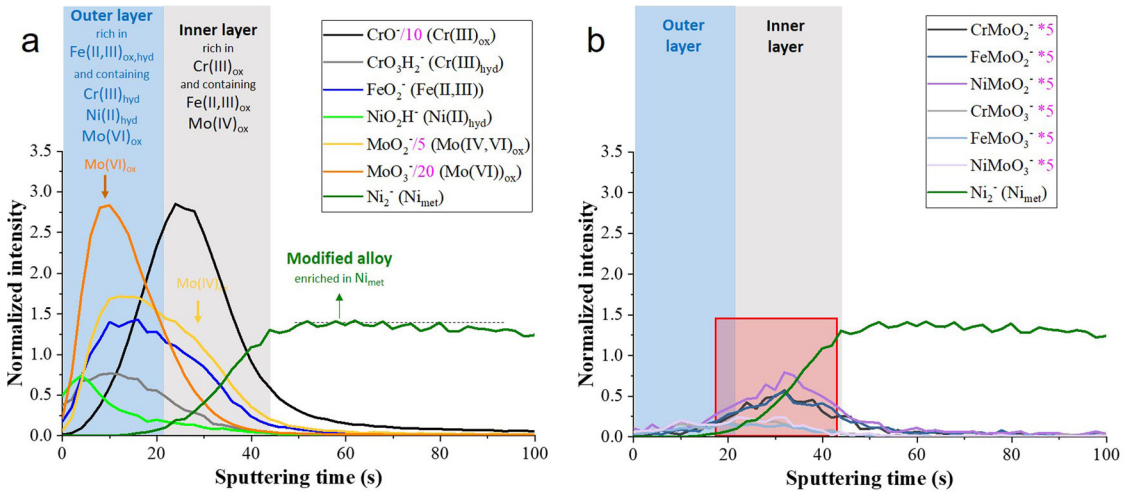

Fig. 5 ToF-SIMS elemental in-depth distribution for passivated $Cr_{25}Fe_{25}Co_5Ni_{40}Mo_5$ surfaces. Passivation was carried out in NaCl-free 0.05 M H_2SO_4 + solution at 0.64 V/SHE for 1 h after stabilization at OCP. **a** Main oxide and hydroxide species constituting the passive films. Adapted from ref. [69]. Copyright owned by authors. **b** Minor mixed $XMoO_n$ (X = Cr, Fe, Ni) oxide species concentrated in the inner layer near the interface with the MPEA substrate.

complementary effects. Its enrichment in the outer layer impedes the deep penetration of the chloride ions, an effect also obtained by Cl-free pre-passivation. When chlorides access the inner barrier layer, Mo counteracts their destabilizing effect by improving the resistance to breakdown of the more susceptible Fe-rich defect sites.

Localization of Mo in bilayer passive oxide films

ToF-SIMS depth profiling was also applied to investigate the in-depth distribution of the Mo oxide species in the passive films formed on such Mo-bearing MPEAs and combined with XPS to study their nature and concentrations[69]. As shown on Fig. 5a for the $Cr_{25}Fe_{25}Co_5Ni_{40}Mo_5$ alloy, the depth distributions of the Mo(IV) and Mo(VI) oxide species are different. The Mo(VI) oxide species, characterized by the MoO_3^- secondary ions, are mostly concentrated in the outer layer of the passive film rich in Cr(III) hydroxide and Fe(II,III) oxide/hydroxide and containing Ni(II) hydroxide. In contrast, the Mo(IV) oxide species, characterized by the MoO_2^- secondary ions, are more homogeneously distributed in depth, and even dominate the Mo content in the inner Cr(III) oxide-rich barrier layer. The peak observed in the outer layer for the MoO_2^- secondary ions may partly result from the fragmentation of the MoO_3^- secondary ions. However, the slower intensity decay of the MoO_2^- secondary ions observed afterwards clearly marks the predominance of Mo(IV) oxide species when at the onset of the transition between outer and inner layers. This difference in depth distribution of the Mo(IV) and Mo(VI) oxide species was also confirmed for $Cr_{15}Fe_{10}Co_5Ni_{60}Mo_{10}$ alloy surfaces passivated in the same conditions[69].

In addition to Mo(IV) and Mo(VI) oxide species, XPS analysis also revealed an additional Mo species characterized by a 5/2–3/2 doublet component observed in the Mo 3d core level region at a binding energy (231.2–234.3 eV) intermediate between those of the Mo(IV) and Mo(VI) components, at 227.8–231.0 and 232.6–235.7 eV, respectively[69]. Such an intermediate Mo species has been previously observed and assigned to hydroxylated Mo(IV)[15,23], Mo(V) oxide[28,71,72], or an intrinsic satellite of Mo(IV) oxide due to final state screening effect[73,74]. From angular XPS analysis[69], it was observed that the Mo(IV) oxide species were located deeper than the Mo(VI) oxide species, in agreement with the Tof-SIMS data (Fig. 5a), and that the intermediate Mo species were located underneath the Mo(IV) oxide species. The intermediate Mo species observed by XPS could thus be an oxide species present in the Cr(III) oxide matrix of the inner barrier layer, including in the Fe-rich defect sites, and carrying a formal charge higher than +4.

Regarding the concentration of the Mo(IV) oxide species, quantification of the XPS relative intensities was carried out using a bilayer model with Mo(IV) assumed to form and interfacial layer between the outer and inner layers as suggested by the peak of the MoO_2^- secondary ions clearly observed after that of the MoO_3^- secondary ions and before that of the CrO^- secondary ions characteristic for the Cr(III) oxide species (Fig. 5a). This resulted in equivalent thicknesses of 0.12 nm at the most for the passivated $Cr_{15}Fe_{10}Co_5Ni_{60}Mo_{10}$ alloy[69]. This corresponds to only fractions of one oxide monolayer suggesting that, even if accumulated at this interface, the Mo(IV) oxide species would not form a dense monolayer fully covering the inner barrier layer. For the intermediate Mo species and assuming their location in the Cr(III) inner barrier layer, their cationic fraction was calculated to be 6 and 19 at. % for the passivated $Cr_{25}Fe_{25}Co_5Ni_{40}Mo_5$ and $Cr_{15}Fe_{10}Co_5Ni_{60}Mo_{10}$ alloys, respectively, which is too high to be consistent with a doping effect of the Cr(III) oxide matrix of the inner layer and rather suggests a mixing effect, including at the Fe-rich oxide defect sites.

The ToF-SIMS depth profiles presented in Fig. 5b supports this view of the minor presence of mixed $XMoO_n$ (X = Cr, Fe, Ni) oxide species in the inner region of the passive film formed on the $Cr_{25}Fe_{25}Co_5Ni_{40}Mo_5$ alloy. Indeed, an intensity maximum is observed near the interface with the substrate for $XMoO_2^-$ and $XMoO_3^-$ secondary ions that would originate from such parent mixed species, with the maxima being more intense for the $XMoO_2^-$ secondary ions. The oxidation state of molybdenum cannot be retrieved from such measurements but this insight is provided by atomistic DFT simulation as discussed below.

Model of the passive oxide film with defect sites cured by Mo

Figure 6 presents the model of passivated CrFeCoNiMo alloy surfaces proposed to account for these observations, and considering the localization of molybdenum at the nanometer scale. Like on passivated stainless steel surfaces, a bilayer structure is formed with the outer exchange layer enriched in Cr(III) hydroxide and containing Fe(II,III) oxide/hydroxide and Ni(II) hydroxide. Molybdenum is enriched as Mo(VI) oxide in this outer layer and its major effect is to impede the deep penetration of chloride ions (Fig. 4), as also observed for stainless steel surfaces[57].

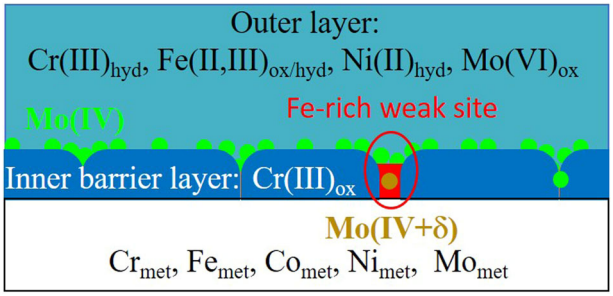

Fig. 6 Model of the duplex passive oxide film formed on CrFeCoNiMo MPEA surfaces. Fe-rich and defect sites of the inner barrier layer are protected against corrosive attack by the local enrichment in Mo(IV + δ) and Mo(IV) oxide species. Adapted from ref. [69]. Copyright owned by authors.

Thus, it contributes to prevent passivity breakdown even in concentrated NaCl-containing aggressive electrolyte (Fig. 3b).

The inner barrier layer is mostly constituted of Cr(III) oxide like on passivated stainless steel surfaces. However, compositional and nanostructural defects are present, originating from the initial growth of the oxide film (Fig. 1). Compositional defects are Fe-rich sites, originating from the failure of the local supply of Cr during the pre-passivation process. Structural defects are mostly intergranular boundaries between the nanometer-size oxide grains produced by the nucleation and growth mechanism of the initial oxide film. These defects may be partially cured by Cr and Mo enrichments observed upon passivation in aqueous solution. However, they may subsist even after reaching a steady-state of passivity in Cl-free environment. The major effect of the Mo(IV) species concentrated at the interface between the outer and inner layers region of the passive film would be to form a (discontinuous) layer protecting these local chemical and structural defects. In this model, Fe-rich defect sites are stabilized by partial substitution or insertion of Mo cations at the surface, subsurface or even in the bulk of their oxide matrix. The DFT simulation discussed hereafter provided atomic insight on how substitutional Mo cures the weak sites in the passive film and thus counteracts the destabilizing effect of chlorides. The intergranular boundaries joining the oxide nanograins, expected to be preferential pathways for atomic transport across the protective inner layer[10], could also be cured by Mo preferentially inserted at these interfaces of the barrier inner layer.

DFT atomistic insights into the role of Mo

Given the complexity of the stratified structure of passivated Cr- and Mo-bearing alloy surfaces and the relative lack of relevant structural details at the atomic scale, assumptions for atomistic modeling must include what appears as the most relevant feature for corrosion protection. For the systems under consideration here, it is the inner layer of the passive film that must be modeled, even though Mo enriched in the outer layer can impede the deep penetration of chloride ions and thus contribute to stabilize passivity. Indeed, the inner layer forms a dense barrier that slows down the atomic transport across the interface and thus drastically limits the exchange current in the passive state thus ensuring the corrosion protection[9,11,75]. Ultimately, this barrier must breakdown and fail to self-repair for localized corrosion to initiate[8–13]. On Fe-based stainless alloys, this inner layer of the passive film is mostly constituted of Cr(III) oxide but can contain compositional defects corresponding to Fe-rich sites, in addition to nanostructural defects. Mo, mostly present as Mo(VI) in the outer layer, is also present as Mo(IV) at the interface with the inner layer and possibly as Mo(IV + δ) in the oxide matrix of the inner layer as discussed above.

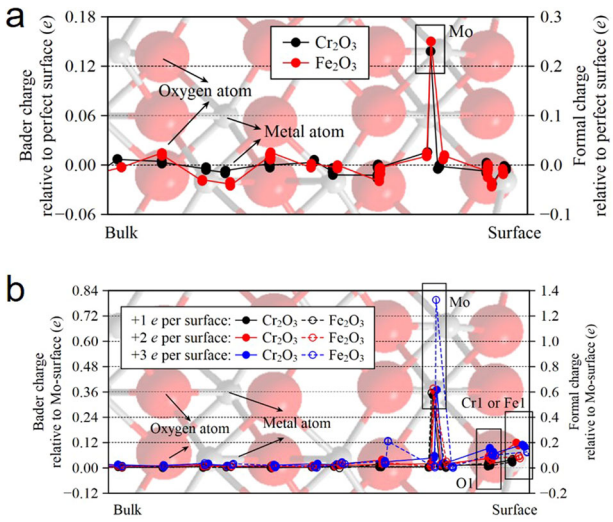

Fig. 7 DFT optimized (0001)-oriented Cr_2O_3 and Fe_2O_3 surfaces with Cr(Fe) substituted by Mo in sub-surface and calculated Bader and formal charges. a Neutral surfaces relative to the Mo-free surfaces. **b** Charged surfaces relative to neutral surfaces. Each point represents an atomic layer whose nature is indicated by the background image of the perfect surface according to the [0001] coordinate. O atoms are in red and metal atoms in gray. Adapted from ref. [76] with permission from Elsevier.

The strategy adopted for atomistic modeling by DFT of the Mo effects was to build periodic systems of an oxide matrix common to chromium and iron oxides, at the surface of which a Cr or Fe atom was substituted by a Mo atom[76]. The different possible sites of replacement were investigated as well as the distributions of charges for the most stable substituted systems. Then, the effects of substitutional Mo on the formation energy of point defects, Cr (or Fe) metal vacancies or O vacancies, at the surface of the oxide matrix were calculated. The corundum structure, common to chromite (Cr_2O_3) and hematite (Fe_2O_3) and terminated by its most stable (0001) surface, was used for modeling, thus enabling direct comparison between oxides of the same structure. DFT + U was applied for the calculations and all details have been reported in a recent paper[76].

Using this approach, it was shown that, on neutral and vacancy-free surfaces, substitution by Mo is always exothermic and the most stable location is in the third metal plane of the (0001)-oriented surface, i.e., in between the first (topmost) and second O planes (Fig. 7). Energetically, this substitution is more favored on Fe_2O_3 than on Cr_2O_3 surfaces. Thus, if both Fe-rich and Cr-rich oxide zones coexist in the inner barrier layer the passive film as discussed above, DFT simulation suggests that Mo may be locally more enriched in the Fe-rich oxide zones than in the Cr-rich oxide zones, which would contribute to cure the Fe-rich weak sites present in the passive film.

The calculated distributions of Bader and formal charges showed that, for neutral (uncharged) systems, the charge on the substitutional Mo is only a little higher than that on the substituted metal atom so that the substitutional Mo can be considered as in +3 oxidation state (Fig. 7a). However, for charged systems, the 1st added positive charge on the Mo-substituted surface is mainly localized on the substitutional Mo which can be considered as in +4 oxidation state. While the 2nd added charge is delocalized, the 3rd added charge is again localized on the substitutional Mo that can reach an intermediate state between +4 and +6 (Fig. 7b). Noteworthy, the localization of the 3rd added charge on the substitutional Mo was only observed on Fe_2O_3. Then, the intermediate Mo(IV + δ) species observed experimentally by XPS may be considered as an indicator of the presence of

Mo-substituted Fe-rich local zones in the inner barrier layer of the passive film (Fig. 6).

Compared to perfect, unsubstituted surfaces, the energy of formation of metal vacancies (Cr or Fe) was always calculated endothermic. However, the presence of substitutional Mo favors the formation of metal atom vacancies, whereas it disfavors the formation of O vacancies or Cr(Fe)-O coupled vacancies. The Mo effect on vacancy formation is also more pronounced on Fe_2O_3 than on Cr_2O_3 surfaces. When a metal atom vacancy is created, the released charge is localized on the substitutional Mo. More charge is localized on Mo in Fe_2O_3 than in Cr_2O_3 defective surfaces, with the substitutional Mo reaching an oxidation state between +4 and +6 on Fe_2O_3 and only +4 on Cr_2O_3. Then, the intermediate Mo(IV + δ) species observed experimentally by XPS could also be a marker of substitutional Mo present in defective Fe-rich local zones with cation vacancies.

The calculations for these Mo-substituted defective systems have implications on how molybdenum could mitigate the breakdown of the inner barrier layer of the passive film. Since substitution by Mo decreases the formation energy of Fe vacancies more significantly than that of Cr vacancies, one can expect the selective dissolution of Fe to be accelerated, and thus iron oxide to be replaced by more stable Mo-substituted chromium oxide in the oxide film. This replacement mechanism would lead to Cr and Mo enrichment, so here the effect of molybdenum is an accelerated selective dissolution of iron, assisted by molybdenum, that would contribute to substitute Fe in the weak sites of the inner barrier layer of the passive film by Mo and Cr, thereby improving the resistance to passivity breakdown.

One of the possible routes leading to passivity breakdown is via the Cl^- ions penetrating the passive oxide films and destabilizing the inner barrier layer[8–13]. Most of the Cl^- ions interacting with the passive film would not access the inner barrier layer thanks to the Mo(VI) oxide species of the outer layer impeding their deep penetration. Still, deep penetration could occur locally leading to interaction of the Cl^- ions with the inner barrier layer and their possible penetration in the oxide matrix via O vacancies. However, DFT simulation suggests that substitution by Mo disfavors the formation of O vacancies in both chromium and iron oxide matrices, and more effectively in Fe_2O_3. This implies that the effect of substitutional Mo in the Fe-rich defect sites would be to increase their resistance against chloride entry in the oxide matrix and thereby Cl-induced passivity breakdown. This effect of molybdenum would complement the acceleration of the selective dissolution of iron induced by substitutional Mo and its replacement by Mo and Cr oxide species, healing the Fe-rich weak sites.

In summary, this comprehensive review of experimental data and simulation obtained recently on passivated stainless steel and Cr-bearing MPEA surfaces by advanced surface analysis and DFT calculations provides both nanometer-scale and atomic-scale insights into the understanding of the role of molybdenum in enhancing the stability of passive films. It shows how Mo, enriched in the nanometer-thick passive film, can combine several effects to enhance the resistance to Cl^--induced passivity breakdown. Enriched as Mo(VI) species in the outer exchange layer of the passive film, Mo acts as a barrier impeding the deep penetration of Cl^- ions and limiting their access to the inner barrier layer. Dispersed as Mo(IV) at the surface of the inner layer, it protects against the entry of Cl^- ions into the defect sites of the Cr(III) oxide barrier. In the Fe-rich compositional defects self-generated by the failure of Cr supply upon initial formation of the barrier layer, molybdenum enhances the selective dissolution of iron and its replacement by Cr(III) and Mo(IV + δ) species. By impeding the formation of O vacancies, it also increases the resistance against chloride entry in the oxide matrix, thereby curing the Fe-rich weak sites that would otherwise be preferential sites for Cl^--induced passivity breakdown.

These combined effects of molybdenum enriched in the chromium oxide-based passive film are essential for preventing passivity breakdown in Cl^- solutions.

DATA AVAILABILITY

The relevant data previously unpublished and discussed herein are available from the corresponding authors.

Received: 18 October 2023; Accepted: 18 December 2023;
Published online: 06 January 2024

REFERENCES

1. Macdonald, D. D. Passivity—the key to our metals-based civilization. *Pure Appl. Chem.* **71**, 951–978 (1999).
2. Schmuki, P. From Bacon to barriers: a review on the passivity of metals and alloys. *J. Solid State Electrochem.* **6**, 145–164 (2002).
3. Olsson, C. O. A. & Landolt, D. Passive films on stainless steels—chemistry, structure and growth. *Electrochim. Acta* **48**, 1093–1104 (2003).
4. Strehblow, H.-H., Maurice, V., Marcus, P. Passivity of Metals, 235–326, in *Corrosion Mechanisms in Theory and Practice*, 3rd edn, (ed Marcus, P.) (CRC Press, Taylor and Francis, 2011).
5. Maurice, V. & Marcus, P. Passive films at the nanoscale. *Electrochim. Acta* **84**, 129–138 (2012).
6. Strehblow, H.-H. Passivity of metals studied by surface analytical methods, a review. *Electrochim. Acta* **212**, 630–648 (2016).
7. Maurice, V. & Marcus, P. Progress in corrosion science at atomic and nanometric scales. *Prog. Mater. Sci.* **95**, 132–171 (2018).
8. Frankel, G. S. Pitting corrosion of metals a review of the critical factors. *J. Electrochem. Soc.* **145**, 2186–2198 (1998).
9. Macdonald, D. D. The point defect model for the passive state. *J. Electrochem. Soc.* **139**, 3434–3449 (1992).
10. Marcus, P., Strehblow, H.-H. & Maurice, V. Localized corrosion (pitting): a model of passivity breakdown including the role of the oxide layer nanostructure. *Corros. Sci.* **50**, 2698–2704 (2008).
11. Macdonald, D. D. The history of the Point Defect Model for the passive state: a brief review of film growth aspects. *Electrochim. Acta* **56**, 1761–1772 (2011).
12. Strehblow, H.-H., Marcus, P. Mechanisms of Pitting Corrosion, 349–393, in *Corrosion Mechanisms in Theory and Practice*, 3rd edn (eds Marcus, P.) (CRC Press, Taylor and Francis, 2011).
13. Soltis, J. Passivity breakdown, pit initiation and propagation of pits in metallic materials–review. *Corros. Sci.* **90**, 5–22 (2015).
14. Frankel, G. S., Li, T. & Scully, J. R. Localized corrosion: passive film breakdown vs pit growth stability. *J. Electrochem. Soc.* **164**, C180–C181 (2017).
15. Olefjord, I., Brox, B. & Jelvestam, U. Surface composition of stainless steels during anodic dissolution and passivation studied by ESCA. *J. Electrochem. Soc.* **132**, 2854–2861 (1985).
16. Marcus, P. & Olefjord, I. Round Robin on combined electrochemical and AES/ESCA characterization of the passive films on Fe-Cr and Fe-Cr-Mo alloys. *Corros. Sci.* **28**, 589–602 (1988).
17. Maurice, V., Yang, W. & Marcus, P. XPS and STM study of passive films formed on Fe-22Cr (1 1 0) single-crystal surface. *J. Electrochem. Soc.* **143**, 1182–1200 (1996).
18. Maurice, V., Yang, W. & Marcus, P. X-ray photoelectron spectroscopy and scanning tunneling microscopy study of passive films formed on (1 0 0) Fe-18Cr-13Ni single-crystal surfaces. *J. Electrochem. Soc.* **145**, 909–920 (1998).
19. Olsson, C.-O. A., Malmgren, S., Gorgoi, M. & Edström, K. Quantifying the metal nickel enrichment on stainless steel. *Electrochem. Solid-State Lett.* **14**, C1 (2011).
20. Keller, P. & Strehblow, H.-H. XPS investigations of electrochemically formed passive layers on Fe/Cr-alloys in 0.5 M H2SO4. *Corros. Sci.* **46**, 1939.e1952 (2004).
21. Maurice, V. et al. Effects of molybdenum on the composition and nanoscale morphology of passivated austenitic stainless steel surfaces. *Faraday Discuss.* **180**, 151–170 (2015).
22. Wang, Z. et al. Mechanisms of Cr and Mo enrichments in the passive oxide film on 316 L austenitic stainless steel. *Front. Mater.* **6**, 232 (2019).
23. Lynch, B. et al. Passivation-induced Cr and Mo enrichments of 316 L stainless steel surfaces and effects of controlled pre-oxidation. *J. Electrochem. Soc.* **167**, 141509 (2020).

24. Wang, Z. et al. XPS and ToF-SIMS investigation of native oxides and passive films formed on nickel alloys containing chromium and molybdenum. *J. Electrochem. Soc.* **168**, 041503 (2021).
25. Lynch, B. et al. An XPS and ToF-SIMS study of the passive film formed on a model FeCrNiMo stainless steel surface in aqueous media after thermal pre-oxidation at ultra-low oxygen pressure. *Appl. Surf. Sci.* **554**, 149435 (2021).
26. Strehblow, H.-H., Passivity of Metals, 271–374, in *Advances in Electrochemical Science and Engineering* (John Wiley & Sons, Ltd, 2002).
27. Olsson, C.-O. A. & Hörnström, S. E. An AES and XPS study of the high alloy austenitic stainless steel 254 SMO® tested in a ferric chloride solution. *Corros. Sci.* **36**, 141–151 (1994).
28. Zhang, X., Zagidulin, D. & Shoesmith, D. W. Characterization of film properties on the Ni-Cr-Mo Alloy C-2000. *Electrochim. Acta* **89**, 814–822 (2013).
29. Marcus, P. & Grimal, J. M. The anodic dissolution and passivation of NiCrFe alloys studied by ESCA. *Corros. Sci.* **33**, 805–814 (1992).
30. Sugimoto, K. & Sawada, Y. The role of molybdenum additions to austenitic stainless steels in the inhibition of pitting in acid chloride solutions. *Corros. Sci.* **17**, 425–445 (1977).
31. Steffen, J. & Hofmann, S. Oxidation of NiCr and NiCrFe alloys at room temperature. *Surf. Interf. Anal.* **11**, 617–626 (1988).
32. Lim, A. S. & Atrens, A. ESCA studies of Ni-Cr alloys. *Appl. Phys. A* **54**, 343–349 (1992).
33. Yu, X. et al. Nonequilibrium solute capture in passivating oxide films. *Phys. Rev. Lett.* **121**, 145701 (2018).
34. Cwalina, K. L. et al. In operando analysis of passive film growth on Ni-Cr and Ni-Cr-Mo alloys in chloride solutions. *J. Electrochem. Soc.* **166**, C3241–C3253 (2019).
35. Sherman, Q. C., Voorhees, P. W. & Marks, L. D. Thermodynamics of solute capture during the oxidation of multicomponent metals. *Acta Mater.* **181**, 584–594 (2019).
36. Mozhi, T. A. et al. The effect of nitrogen on the sensitization of AISI 304 stainless steel. *Corrosion* **41**, 555–559 (1985).
37. Marcus, P. On some fundamental factors in the effect of alloying elements on passivation of alloys. *Corros. Sci.* **36**, 2155–2158 (1994).
38. Rockel, M. B. & Renner, M. Pitting, crevice and stress corrosion resistance of high chromium and molybdenum alloy stainless steels. *Werkst. Korros.* **35**, 537–542 (1984).
39. Ilevbare, G. O. & Burstein, G. T. The role of alloyed molybdenum in the inhibition of pitting corrosion in stainless steels. *Corros. Sci.* **43**, 485–513 (2001).
40. Newman, R. C. The dissolution and passivation kinetics of stainless alloys containing molybdenum—1. Coulometric studies of Fe-Cr and Fe-Cr-Mo alloys. *Corros. Sci.* **25**, 331–339 (1985).
41. Newman, R. C. The dissolution and passivation kinetics of stainless alloys containing molybdenum—II. Dissolution kinetics in artificial pits. *Corros. Sci.* **25**, 341–350 (1985).
42. Vukasovich, M. S. & Farr, J. P. G. Molybdate in corrosion inhibition—a review. *Polyhedron* **5**, 551–559 (1986).
43. Shams El Din, A. M. & Wang, L. Mechanism of corrosion inhibition by sodium molybdate. *Desalination* **107**, 29–43 (1996).
44. Li, X., Deng, S. & Fu, H. Sodium molybdate as a corrosion inhibitor for aluminium in H3PO4 solution. *Corros. Sci.* **53**, 2748–2753 (2011).
45. Kaneko, M. & Isaacs, H. S. Effects of molybdenum on the pitting of ferritic- and austenitic-stainless steels in bromide and chloride solutions. *Corros. Sci.* **44**, 1825–1834 (2002).
46. Alshamsi, A. S. Corrosion of heat-treated 304SS in the presence of molybdate ions in hydrochloric acid. *Int. J. Electrochem. Sci.* **8**, 591–605 (2013).
47. Bojinov, M. et al. Influence of molybdenum on the conduction mechanism in passive films on iron–chromium alloys in sulphuric acid solution. *Electrochim. Acta* **46**, 1339–1358 (2001).
48. Hashimoto, K., Asami, K. & Teramoto, K. An X-ray photo-electron spectroscopic study on the role of molybdenum in increasing the corrosion resistance of ferritic stainless steels in HCl. *Corros. Sci.* **19**, 3–14 (1979).
49. Horvath, J. & Uhlig, H. Critical potentials for pitting corrosion of Ni, Cr-Ni, Cr-Fe, and related stainless steels. *J. Electrochem. Soc.* **115**, 791–796 (1968).
50. Tan, M.-W., Akiyama, E., Kawashima, A., Asami, K. & Hashimoto, K. The effect of air exposure on the corrosion behavior of amorphous Fe-8Cr-Mo-13P-7C alloys in 1 M HCl. *Corros. Sci.* **37**, 1289–1301 (1995).
51. Lee, J.-B. Effects of alloying elements, Cr, Mo and N on repassivation characteristics of stainless steels using the abrading electrode technique. *Mater. Chem. Phys.* **99**, 224–234 (2006).
52. Elbiache, A. & Marcus, P. The role of molybdenum in the dissolution and the passivation of stainless steels with adsorbed sulphur. *Corros. Sci.* **33**, 261–269 (1992).
53. Pardo, A. et al. Effect of Mo and Mn additions on the corrosion behaviour of AISI 304 and 316 stainless steels in H2SO4. *Corros. Sci.* **50**, 780–794 (2008).
54. Pardo, A. et al. Pitting corrosion behaviour of austenitic stainless steels–combining effects of Mn and Mo additions. *Corros. Sci.* **50**, 1796–1806 (2008).
55. Sun, Y. -T., Tan, X., Lei, L. -L., Li, J. & Jiang, Y. -M. Revisiting the effect of molybdenum on pitting resistance of stainless steels. *Tungsten* **3**, 329–337 (2021).
56. Yamamoto, T. et al. Depassivation–repassivation behavior of type-312L stainless steel in NaCl solution investigated by the micro-indentation. *Corros. Sci.* **51**, 1545–1553 (2009).
57. Wang, Z., Seyeux, A., Zanna, S., Maurice, V. & Marcus, P. Chloride-induced alterations of the passive film on 316 L stainless steel and blocking effect of prepassivation. *Electrochim. Acta* **329**, 135159 (2020).
58. Vignal, V., Olive, J. M. & Desjardins, D. Effect of molybdenum on passivity of stainless steel chloride media using ex situ near field microscopy observations. *Corros. Sci.* **41**, 869–884 (1999).
59. Wang, L., Seyeux, A. & Marcus, P. Ion transport mechanisms in the oxide film formed on 316 L stainless steel surfaces studied by ToF-SIMS with 18O2 isotopic tracer. *J. Electrochem. Soc.* **167**, 101511 (2020).
60. Lloyd, A. C., Noël, J. J., McIntyre, S. & D.W. Shoesmith, C. R. Mo and W alloying additions in Ni and their effect on passivity. *Electrochim. Acta* **49**, 3015–3027 (2004).
61. Henderson, J. D., Li, X., Shoesmith, D. W., Noël, J. J. & Ogle, K. Molybdenum surface enrichment and release during transpassive dissolution of Ni-based alloys. *Corros. Sci.* **147**, 32–40 (2019).
62. Ma, L., Wiame, F., Maurice, V. & Marcus, P. Stainless steel surface structure and initial oxidation at nanometric and atomic scales. *Appl. Surf. Sci.* **494**, 8–12 (2019).
63. Ma, L., Wiame, F., Maurice, V. & Marcus, P. Origin of nanoscale heterogeneity in the surface oxide film protecting stainless steel against corrosion. *npj Mater. Degrad.* **3**, 1–9 (2019).
64. Ma, L., Lynch, B., Wiame, F., Maurice, V. & Marcus, P. Nanoscale early oxidation mechanisms of model FeCrNi austenitic stainless steel surfaces at room temperature. *Corros. Sci.* **190**, 109653 (2021).
65. Lynch, B., Wiame, F., Maurice, V. & Marcus, P. XPS study of oxide nucleation and growth mechanisms on a model FeCrNiMo stainless steel surface. *Appl. Surf. Sci.* **575**, 151681 (2022).
66. Yue, X. Q. et al. Synchrotron-based near ambient-pressure X-ray photoelectron spectroscopy and electrochemical studies of passivation behavior of N- and V-containing martensitic stainless steel. *Corros. Sci.* **214**, 111018 (2023).
67. Neupane, S. et al. Can we enhance passivity with a surface finish? Spectroscopic and electrochemical analysis on 316 L stainless steel. *J. Electrochem. Soc.* **169**, 011505 (2022).
68. Wang, X. et al. Enhanced passivity of Cr-Fe-Co-Ni-Mo multi-component single-phase face-centred cubic alloys: design, production and corrosion behaviour. *Corros. Sci.* **200**, 110233 (2022).
69. Wang, X. et al. Origin of enhanced passivity of Cr-Fe-Co-Ni-Mo multi-principal element alloy surfaces. *npj Mater. Degrad.* **7**, 13 (2023).
70. Wang, X. et al. Effects of chloride ions on passive oxide films formed on Cr-Fe-Co-Ni(-Mo) multi-principal element alloy surfaces. *J. Electrochem. Soc.* **170**, 041506 (2023).
71. Clayton, C. R. & Lu, Y. C. Electrochemical and XPS evidence of the aqueous formation of Mo_2O_5. *Surf. Interf. Anal.* **14**, 66–70 (1989).
72. Eidhagen, J. et al. Synchrotron XPS and electrochemical study of aging effect on passive film of Ni alloys. *J. Electrochem. Soc.* **170**, 021506 (2023).
73. Gulino, A., Parker, S., Jones, F. H. & Egdell, R. G. Influence of metal–metal bonds on electron spectra of MoO_2 and WO_2. *J. Chem. Soc. Faraday Trans.* **92**, 2137–2141 (1996).
74. Scanlon, D. O. et al. Theoretical and experimental study of the electronic structures of MoO3 and MoO2. *J. Phys. Chem. C.* **114**, 4636–4645 (2010).
75. Seyeux, A., Maurice, V. & Marcus, P. Oxide film growth kinetics on metals and alloys: I. physical model. *J. Electrochem. Soc.* **160**, C189–C196 (2013).
76. Huang, X., Costa, D., Diawara, B., Maurice, V. & Marcus, P. Atomistic insights on enhanced passivity: DFT study of substitutional Mo on Cr2O3 and Fe2O3 surfaces. *Corros. Sci.* **224**, 111543 (2023).

ACKNOWLEDGEMENTS

This work was supported by the European Research Council (ERC) under the European Union's Horizon 2020 research and innovation program (ERC Advanced Grant Agreement No 741123: Corrosion Initiation Mechanisms at the Nanoscale and Atomic Scale). Dimitri Mercier, Dominique Costa, Frédéric Wiame, Sandrine Zanna, Antoine Seyeux, Lorena H. Klein, Boubakar Diawara, Li Ma, Zuocheng Wang, Ben Lynch, Xueying Wang, Xian Huang, Eirini-Maria Paschalidou, Shova Neupane are acknowledged with thanks for their contributions to the production of the original data previously published and further discussed herein.

AUTHOR CONTRIBUTIONS

This review was conceived by V.M. and P.M. V.M. wrote the first draft, reviewed by P.M. V.M. contributed to funding acquisition and P.M. both funding acquisition and project management. Both authors approved the final version.

COMPETING INTERESTS

The authors declare no competing interests.

ADDITIONAL INFORMATION

Correspondence and requests for materials should be addressed to Vincent Maurice or Philippe Marcus.

Reprints and permission information is available at http://www.nature.com/reprints

Publisher's note Springer Nature remains neutral with regard to jurisdictional claims in published maps and institutional affiliations.

Open Access This article is licensed under a Creative Commons Attribution 4.0 International License, which permits use, sharing, adaptation, distribution and reproduction in any medium or format, as long as you give appropriate credit to the original author(s) and the source, provide a link to the Creative Commons license, and indicate if changes were made. The images or other third party material in this article are included in the article's Creative Commons license, unless indicated otherwise in a credit line to the material. If material is not included in the article's Creative Commons license and your intended use is not permitted by statutory regulation or exceeds the permitted use, you will need to obtain permission directly from the copyright holder. To view a copy of this license, visit http://creativecommons.org/licenses/by/4.0/.

© The Author(s) 2024